2018 IEEE-RAS 18th International Conference on Humanoid Robots (Humanoids)
Beijing, China, November 6-9, 2018

Optimization Framework of Humanoid Walking Pattern for Human Motion Retargeting

Shimpei Masuda[1,2], Ko Ayusawa[1] Eiichi Yoshida[1,2]

***Abstract*— In this paper, we propose a novel method for retargeting human movements including the steps taken by a humanoid robot. For applications, such as wearable device evaluation by a humanoid, it is necessary to reproduce the original human motions as closely as possible and to generate motions that can be realized on a real robot without the robot losing its balance. The proposed method features the optimization framework that integrates the walking pattern generation based on the linear inverted pendulum model whose parameters are optimized to ensure both human likeness and feasibility of the generated motions. The effectiveness of the retargeting method is validated by experiments that reproducing the measured human working motion on the humanoid HRP-4.**

I. Introduction

Along with an increase in workers, we are experiencing an increasing demand for wearable assistive devices, such as power-assisted suits for amplifying human strength. To develop and spread wearable assistive devices, we need a method for quantitatively evaluating the performance of each device. As a framework for obtaining quantitative evaluation, a method using a humanoid robot has been proposed [1]. In this framework, humanoid robot performs human motions with and without an assistive device, and the internal load is measured from the internal sensors. Also, this framework is expected to solve the problem of motion repeatability and ethics. Nabeshima et al. have established standards in Japan for assistive devices that are attached to the waist [2]. However, this evaluation framework has not been realized for assistive devices that support walking or other motions that involve taking steps. One reason is that it is difficult to generate robot motions that mimic dynamic human motions such as walking, which involve changes in the foot placements. Furthermore, it is necessary to realize the generated motion under various disturbances and modeling errors.

Some studies have already reported the reproduction of human motions (measured by motion capture systems) for life-sized humanoid robots. Nakaoka et al. defined the task primitives and parameters for lower body movements and reproduced a measured Japanese dance on HRP-2 [3]. For HRP-2, Ramos et al. succeeded in reproducing the dance motion including the leg movements by considering the consistency of the dynamics [4]. Miura et al. generated a turning motion for the humanoid HRP-4 by using the measured human motions [5]. Ishiguro et al. realized real-time motion reproduction as a master–slave system [6]. Although these approaches can generate feasible motions efficiently, they are not aimed at precise preservation of motion characteristics such as the angle trajectory of the specific joint. When converting the captured human motions into the feasible one for the humanoids, several studies have been reported such as Dynamics Filter proposed by Yamane et al[7]. Though the method can generate the motion which has high reproducibility and dynamically consistent, the lack of locomotion control leads instability of biped motion of a real humanoid robot.

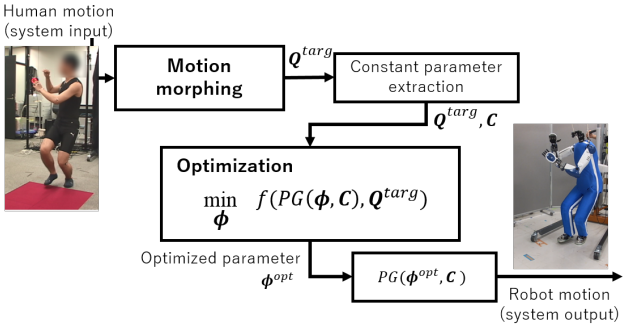

Fig. 1. Overview of motion reproduction method

In this paper, we propose a novel method of reproducing the walking motions of humans by a humanoid robot while considering the stability issue of locomotion toward the the applications in the real robot. We introduce a retargeting framework that integrates optimization and pattern generation. We constructed a walking pattern generator that outputs walking motions based on the linear inverted pendulum model (LIPM) [8], whose parameters are optimized to achieve the target human motions while satisfying both the reproducibility and feasibility. The pattern generated according to LIPM is compatible with stabilization control using LIPM [9]. Therefore, the combination leads the high performance against disturbances in the real world. According to similar concept, Kondo et al. optimized small gait parameters by genetic algorithm and reproduced measured human walking motion by using WABIAN-2 [10]. In our method, many parameters including the foot-print and waist pose can be optimized in order to enhance the reproducibility of original human motion. On the other hand, more than 60 parameters need to be optimized. To solve the nonlinear problem, the gradient of the cost function need to be computed accurately. Since the function including pattern gen-

*This work was partly supported by JSPS Grant-in-Aid for Scientific Research (A) Number 17H00768, and by JSPS Grant-in-Aid for Scientific Research (B) Number 18H03315.

S. Masuda and E.Yoshida are with [1]University of Tsukuba, Japan. S. Masuda, K. Ayusawa and E. Yoshida are with [2]CNRS-AIST JRL (Joint Robotics Laboratory), UMI3218/RL, Tsukuba, Japan. Corresponding author: S. Masuda s1720858@s.tsukuba.ac.jp

erator has complicated structure, we applied the automatic differentiation (AD) technique. We also built a generator that can generate the motion algorithmically from the parameters to apply AD. The motion retargeting method was validated by an experiment, which reproduced the measured human working motion on the humanoid HRP-4 [11].

II. Retargeting using Optimization and LIPM base pattern generation

A. Overview

Figure 1 provides an overview of our retargeting system. The system takes a measured human motion clip as an input and outputs the retargeted robot motion pattern which is dynamically consistent and stable. The system is mainly composed of a motion morphing part and an optimization part. The motion morphing part converts the human motion into a robot motion. The converted motion is used as a reference in latter part. Then, the optimization part then optimizes the parameters of the pattern generator based on LIPM to minimize the difference between the generated motion and the reference. Finally, the overall system generates the motion pattern with the acquired optimal parameters.

B. Motion morphing for generating reference robot motion

The body structure of a human actor and a humanoid robot are quite different. We employed the method proposed by Ayusawa et al. [12] for scaling the body structure; however, this method only considers the kinematic feasibility. In the motion optimization part, the robot motion that was morphed from human motion is set as the reference.

C. Motion optimization using LIPM based pattern generation

The direct optimization of motions that involve several footsteps is difficult, especially for following: 1) The floor contact state is discrete information that is difficult to use in mathematical formulations. 2) Complex constraints are necessary, for example, for tracking the targeted zero-moment point (ZMP) trajectory. We address these problems by using optimization including the walking pattern generation based on LIPM [8].

When the humanoid robot's CoM moves in the horizontal plane and the angular momentum around CoM is zero, its dynamics can be represented as a linear inverted pendulum as follows:

$$\ddot{x} = \frac{g}{z_c}(x - p) \tag{1}$$

where x is position of CoM; z_c is the vertical height of CoM; p is position of ZMP; and g is the gravity acceleration. When a footprint (the floor contact positions and timings) is given as the input of the generator, it can determine a ZMP trajectory based on some assumptions. For example, ZMP is set at the center of the sole during a single supporting phase, and so on. Then, a CoM trajectory that tracks the ZMP trajectory is calculated from (1). The walking pattern is calculated from the foot trajectory determined from the footprint and the waist and the upper body posture trajectory that tracks the CoM trajectory [13]. We have extended this LIPM-based walking pattern generator that can generate various walking motions.

Let $\boldsymbol{q}^{targ}$ and $\boldsymbol{q}^{gen}$ be the generalized coordinates of the robot as follows:

$$\boldsymbol{q}^{targ} = [\ p_{base}^{targ} \quad R_{base}^{targ} \quad \boldsymbol{\theta}^{targ}\ ] \tag{2}$$

$$\boldsymbol{q}^{gen} = [\ p_{base}^{gen} \quad R_{base}^{gen} \quad \boldsymbol{\theta}^{gen}\ ] \tag{3}$$

where p_{base}^{targ} and p_{base}^{gen} are the position of baselink, R_{base}^{targ} and R_{base}^{gen} are the rotation of the baselink, and $\boldsymbol{\theta}^{targ}$ and $\boldsymbol{\theta}^{gen}$ are the joint angle of whole body. At each time instance $t_1, t_2, \cdots, t_{N_T}$, let $\boldsymbol{q}_t^{targ}$ and $\boldsymbol{q}_t^{gen}$ $(1 \leq t \leq N_T)$ be the reference and the generated robot postures, respectively. Let the generated motion pattern for the humanoid be $\boldsymbol{Q}^{gen} (\triangleq [\boldsymbol{q}_1^{gen} \cdots \boldsymbol{q}_{N_T}^{gen}]) = PG(\boldsymbol{\phi}, \boldsymbol{C})$, where $\boldsymbol{\phi}$ is the set of variable parameters for pattern generation (such as z_c in (1)), and $\boldsymbol{C}$ is the set of constant parameters. Assuming that the pattern generator has sufficient DoF to reproduce the target motion, the motion reproduction can be expressed as an optimization problem of the parameters of PG as follows:

$$\min_{\phi} \quad f(PG(\boldsymbol{\phi}, \boldsymbol{C}), \boldsymbol{Q}^{targ}) \tag{4}$$

where $\boldsymbol{Q}^{targ} \triangleq [\boldsymbol{q}_1^{targ} \cdots \boldsymbol{q}_{N_T}^{targ}]$ is the reference motion, and f is the error function for calculating the difference between $\boldsymbol{Q}^{gen}$ and $\boldsymbol{Q}^{targ}$. In this paper, we used the sum of squared error of the angles of the hip and the knee joints as objective function. The equality or inequality constraints are handled as the penalty terms in the objective function. The nonlinear optimization problem can be solved by the Quasi-Newton method or another such method, but a gradient is required. We employed AD [14] to compute the accurate gradient of the whole system from motion pattern generation to motion evaluation. Though AD requires time and effort from a naive software implementation, it can quickly compute the derivatives with high accuracy in contrast to numerical differentiation.

The details of pattern generator improvements will be described in Section III.

III. Pattern generator for motion optimization with AD

A. Overview

Figure 2 shows a diagram for the implementation of a pattern generator. The steps in the pattern generator process are as follows:

1) Determine the reference ZMP trajectory and the foot motion.
2) Calculate a baselink posture trajectory and generate the whole-body motion once.
3) Compensate for the ZMP error by modifying the baselink trajectory and output the motion pattern.

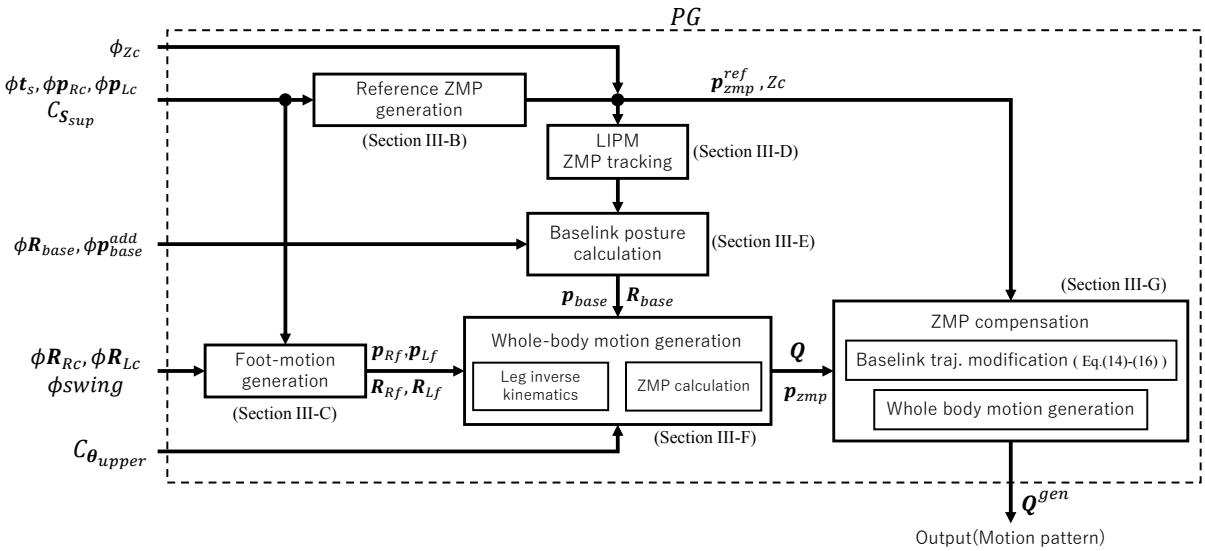

Fig. 2. Implementation of the pattern generator PG

B. Reference ZMP generation

First, we define $C_{\boldsymbol{S}_{sup}}$ as a sequence of the support state in the whole motion. It is a constant parameter and is measured from the reference motion. Also $\phi_{\boldsymbol{t}_s} = [t_{s,1} \cdots t_{s,N_{t_s}}]$ is defined as the change timings of the support-state sequence. $\phi_{\boldsymbol{p}_{Rc}} = [p_{Rc,1} \cdots p_{Rc,N_{Rc}}]$ and $\phi_{\boldsymbol{p}_{Lc}} = [p_{Lc,1} \cdots p_{Lc,N_{Lc}}]$ are defined as the positions for each floor contact of each foot (R indicates right, and L indicates left). N_{t_s}, N_{Rc} and N_{Lc} are the number of each parameter and is determined from $C_{\boldsymbol{S}_{sup}}$. The reference ZMP trajectory $\boldsymbol{p}^{ref}_{zmp} \triangleq [p^{ref}_{zmp,1} \cdots p^{ref}_{zmp,N_T}]$ is generated from these parameters as follows:

$$\boldsymbol{p}^{ref}_{zmp} = f^{ref}_{zmp}(C_{\boldsymbol{S}_{sup}}, \phi_{\boldsymbol{t}_s}, \phi_{\boldsymbol{p}_{Rc}}, \phi_{\boldsymbol{p}_{Lc}}) \tag{5}$$

The trajectory is generated by the interpolation of the via point determined according to footprint parameters: $\phi_{\boldsymbol{t}_s}$, $\phi_{\boldsymbol{p}_{Rc}}$ and $\phi_{\boldsymbol{p}_{Lc}}$. The interpolation of the two adjacent via points can be formulated as follows:

$$a = (1 - \mu)a_0 + \mu a_1 \tag{6}$$

$$\mu = (1 - cos(\pi\tau))/2 \tag{7}$$

where τ is the normalized time between the time instances corresponding to the two adjacent via points, and a is the interpolated value from a_0 and a_1 at τ. This interpolation is employed through all via points to avoid overshooting and to set the velocity to zero near the via point. Figure 3 shows the implementation of (5) for the X-axis (the sagittal axis) and the Y-axis (the frontal axis);this figure also gives an example of walking four steps by stepping out with the right foot. In Figure 3, the red points specify the via points, and the green line is interpolated as the ZMP trajectory. "D" in $C_{\boldsymbol{S}_{sup}}$ indicates the double support phase and "R" and "L" indicate the single support phase with the right foot or the left foot. We used the constant transition time of ZMP in the first swing and the last landing time to/from the adjacent ZMP reference was experimentally set to $t_b = 0.1$ s.

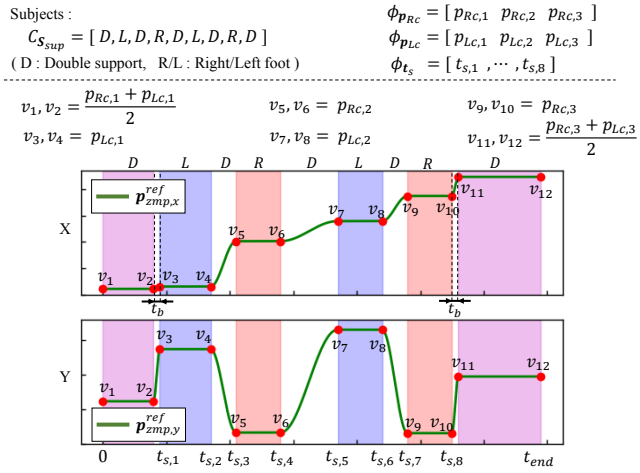

Fig. 3. Procedure of reference ZMP trajectory generation.

C. Foot-motion generation

The foot motion is determined in a manner similar to the ZMP trajectory, as given in the previous subsection. Let $\phi_{\boldsymbol{R}_{Rc}} = [R_{Rc,1} \cdots R_{Rc,N_{Rc}}]$ and $\phi_{\boldsymbol{R}_{Lc}} = [R_{Lc,1} \cdots R_{Lc,N_{Lc}}]$ be the rotation of the right foot and the left foot, respectively. The foot-motion generation defined by the function f_{foot}, to compute $\boldsymbol{p}_{Rf}$,$\boldsymbol{p}_{Lf}$,$\boldsymbol{R}_{Rf}$,$\boldsymbol{R}_{Lf}$ is as follows:

$$\begin{aligned} &\boldsymbol{p}_{Rf}, \boldsymbol{R}_{Rf}, \boldsymbol{p}_{Lf}, \boldsymbol{R}_{Lf} = \\ &\quad f_{foot}(\phi_{\boldsymbol{S}_{sup}}, \phi_{\boldsymbol{t}_s}, \phi_{\boldsymbol{p}_{Rc}}, \phi_{\boldsymbol{R}_{Rc}}, \phi_{\boldsymbol{p}_{Lc}}, \phi_{\boldsymbol{R}_{Lc}}, \phi_{swing}) \end{aligned} \tag{8}$$

where ϕ_{swing} is the height of the swing foot during the walking motion at half of the swing period. Figure 4 shows the implementation of the foot-motion generation given in

(8) for the X-axis (sagittal axis) and the Z-axis (vertical axis). Start timing of the swing and the landing timing are extracted from $\phi_{\boldsymbol{t}_s}$ with reference to $C_{\boldsymbol{S}_{sup}}$ so that the timing of each via point is determined. The trajectory is generated by the interpolation formula given in (7). The procedure implemented on the Y-axis (the frontal axis) and the rotation trajectory were also same as that for the X-axis.

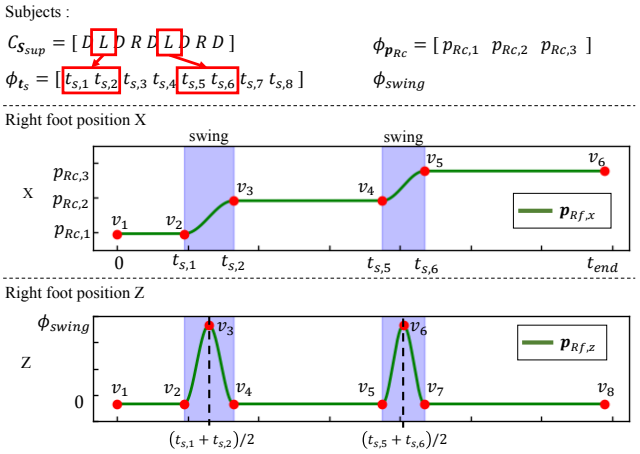

Fig. 4. Procedure for foot-motion generation.

D. LIPM ZMP tracking

In each sagittal and frontal plane, the CoM trajectory tracking the ZMP trajectory is obtained from the discretized LIPM as follows [15]:

$$\boldsymbol{x}_{com} = \boldsymbol{A}^{-1}\boldsymbol{x}_{zmp} \tag{9}$$

$\boldsymbol{A}$, the $N_T \times N_T$ matrix, is defined as follows:

$$\boldsymbol{A} = \begin{pmatrix} a+b & c & 0 & & & \\ a & b & c & \ddots & & \\ & & & \ddots & & \\ & & & \ddots & a & b & c \\ & & & & 0 & a & b+c \end{pmatrix}$$

$$\begin{aligned} a &= -z_c/(g\Delta t^2) \\ b &= -2z_c/(g\Delta t^2) + 1 \\ c &= -z_c/(g\Delta t^2) \\ z_c &= \phi z_c \end{aligned}$$

In this implementation, the CoM position is assumed to be close to the position of the waist link (i.e. the baselink). The trajectory of the baselink is computed as follows:

$$\boldsymbol{p}_{base,x} = \boldsymbol{A}^{-1}\boldsymbol{p}^{ref}_{zmp,x} \tag{10}$$
$$\boldsymbol{p}_{base,y} = \boldsymbol{A}^{-1}\boldsymbol{p}^{ref}_{zmp,y} \tag{11}$$
$$\boldsymbol{p}_{base,z} = \phi z_c \tag{12}$$

E. Baselink posture calculation

This component adds additional vertical movement to $\boldsymbol{p}_{base}$ as follows:

$$\boldsymbol{p}_{base,z} = \phi z_c + f_{spline}(\phi_{\boldsymbol{p}^{add}_{base}}) \tag{13}$$

where the function f_{spline} calculates the trajectory by uniform B-spline of order 3, and the argument is the control point of the spline. Let $\boldsymbol{R}_{base}$, the rotational trajectory of the baselink, be given as follows:

$$\boldsymbol{R}_{base} = \boldsymbol{R}_{rpy}(f^{rpy}_{spline}(\phi_{\boldsymbol{R}_{base}})) \tag{14}$$

where f^{rpy}_{spline} calculates three spline trajectories in the same as (13), and function $\boldsymbol{R}_{rpy}(\cdot)$ calculates a rotation matrix with given roll pitch yaw angles.

F. Whole-body motion generation

The joint angles of each leg are calculated from the baselink posture trajectory and each foot trajectory by using inverse kinematics (IK). Here, analytical IK is possible because each leg of HRP-4 has only six DoFs and the axis of three DoFs on the waist are orthogonal. Let $\boldsymbol{\theta}_{Rleg}$ and $\boldsymbol{\theta}_{Lleg}$ be the calculated joint angles of each leg from $\boldsymbol{p}_{Rf}, \boldsymbol{R}_{Rf}, \boldsymbol{p}_{Lf}, \boldsymbol{R}_{Lf}$, $\boldsymbol{p}_{base}$ and $\boldsymbol{R}_{base}$. When given a positional relationship between waist and foot that can not be realized, we clip the norm of foot-baselink and the error is considered in the optimization process.

In this implementation, the joint angle trajectory of the upper body is set to the reference motion received as the parameter $C_{\boldsymbol{\theta}_{upper}}$. Here, $\boldsymbol{Q} \triangleq [\boldsymbol{q}_1 \cdots \boldsymbol{q}_{N_T}]$ is defined as the motion pattern , where $\boldsymbol{q} = [\;p_{base}\quad R_{base}\quad \boldsymbol{\theta}\;]$ and $\boldsymbol{\theta} = [\;\boldsymbol{\theta}_{Rleg}\quad \boldsymbol{\theta}_{Lleg}\quad \boldsymbol{\theta}_{upper}\;]$.

After computing the trajectory generalized coordinate, ZMP can be computed by the whole-body dynamics, where the generalized velocity and acceleration are computed by the numerical differentiation of $\boldsymbol{Q}$. Let $\boldsymbol{p}_{zmp}$ be the computed ZMP trajectory.

G. ZMP compensation

Because of the assumptions made for LIPM and the use of CoM as the baselink, the result of $\boldsymbol{p}_{zmp}$ can have an error from the reference $\boldsymbol{p}^{ref}_{zmp}$. To compensate for the error, the baselink trajectory $\boldsymbol{p}_{base}$ is modified according to the ZMP error as follows:

$$\Delta\boldsymbol{p}_{zmp} = \boldsymbol{p}_{zmp} - \boldsymbol{p}^{ref}_{zmp} \tag{15}$$
$$\Delta\boldsymbol{p}_{base,x} = \boldsymbol{A}^{-1}\Delta\boldsymbol{p}_{zmp,x} \tag{16}$$
$$\Delta\boldsymbol{p}_{base,y} = \boldsymbol{A}^{-1}\Delta\boldsymbol{p}_{zmp,y} \tag{17}$$

where $\boldsymbol{A}$ is the same matrix in (9). The modified baselink position trajectory $\boldsymbol{p}^{gen}_{base}$ is $\boldsymbol{p}^{gen}_{base} = \boldsymbol{p}_{base} + \Delta\boldsymbol{p}_{base}$.

Finally, the output motion pattern $\boldsymbol{Q}^{gen}$ is calculated from the modified $\boldsymbol{p}^{gen}_{base}$ by the whole-body motion generator described in Section III-F.

IV. Experiments

This section presents the results of the experiment to verify the effectiveness of the proposed system.

A. Experiment setup

The left side of Fig.5 shows the human-sized humanoid robot HRP-4. The geometric parameter designs, such as link lengths, were based on the average Japanese female; the height and weight of HRP-4 is almost 155 cm and 40 kg, respectively. The right side of Fig.5 shows the joint configuration of HRP-4. The total number of DoFs of the robot is 37. Joints were added to the toes and to the roll axis of the waist link from the original HRP-4. In this experiment, the toe joints and the hand joints were fixed and unused.

While executing the motion pattern, the joint position controller at each joint tracks the joint angle trajectory. The robot is affected by various disturbances (such as a deformation of some rubbers for shock absorbing on the ankle) and some modeling errors; therefore the stabilization controller is needed. For the stabilization controller, we used an implementation of the LIPM-based stabilization control method that was proposed by Kajita et al. [9].

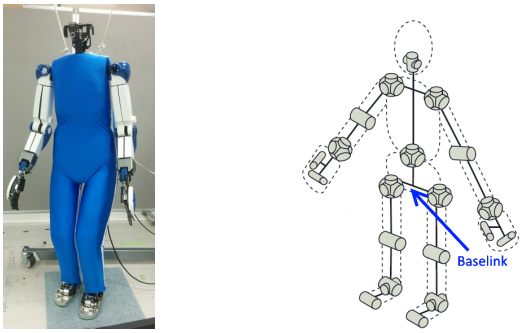

Fig. 5. Overview of HRP-4 (left) and joint configuration (right).

B. Experiment for working motion retargeting

Experiments have been conducted by assuming the case of tasks requiring devices wearable on the lower body. We selected the inspection task in a half-sitting posture as the target motion and measured it by motion capture system (Motion Analysis). The motion is approximately for 6 s and involved four steps. Snapshots of the captured motion are shown at the top of Fig.6. The whole-body motion $\boldsymbol{Q}^{targ}$ was generated as described in Section II-B.

One of our goal is to evaluate the assistive device that performs according to the joint angles of the lower body. In this paper, we used the error of the angles of the hip joints and the knee joints as evaluation that to be minimized. The optimization problem is therefore formulated as follows:

$$
\begin{aligned}
\min_{\boldsymbol{\phi}} \quad & \frac{1}{N_T}\sum_{t=1}^{N_T}\Big(\ ||\boldsymbol{\theta}^{targ}_{hip,t} - \boldsymbol{\theta}^{gen}_{hip,t}||^2 \\
& \qquad + ||\theta^{targ}_{knee,t} - \theta^{gen}_{knee,t}||^2 \\
& \qquad + \omega_{com}||\phi_{z_c} - p_{com,z,t}||^2 \\
& \qquad + \omega_{\mathrm{IK}}||p_{foot,t} - p^{*}_{foot,t}||^2\Big) \\
& + \omega_{fc_k}\sum_{k}||\phi^{init}_{fc,k} - \phi_{fc,k}||^2 \\
\text{subject to} \quad & \phi_{min} \le \phi \le \phi_{max}
\end{aligned}
\tag{18}
$$

where $\boldsymbol{\theta}^{gen}_{hip,t}$ are the three joint angles of the each hip joint extracted from $\theta^{gen}_{Rleg,t}$ and $\theta^{gen}_{Lleg,t}$, and $\theta^{gen}_{knee,t}$ is the knee joint angle. In the problem (18), the constraint conditions excluding the boundary constraint are considered as the penalty term. Also, $\boldsymbol{p}_{com} = [p_{com,1} \cdots p_{com,N_T}]$ is the CoM trajectory of the generated motion, and $p^{*}_{foot,t} \quad (foot = Rf, Lf)$ is the actual foot position calculated by forward kinematics of the generated motion. The weights ω_{com} and ω_{IK} in the cost function in (18) are for the vertical CoM motion and the IK error, respectively, and are empirically set to 100 and 2000, respectively. $\omega_{fc} \quad (fc = \boldsymbol{t}_s, \boldsymbol{p}_{Rc}, \boldsymbol{p}_{Lc}, \boldsymbol{R}_{Rc}, \boldsymbol{R}_{Lc})$ is the weight of the penalty term which constraints the change of the parameter relating to the foot-print to the adjustment, and are set to $\omega_{fc_k} = 0.4$ for $\phi_{\boldsymbol{t}_s}$ and $\omega_{fc_k} = 4.0$ for other foot-print parameters. The parameters to be optimized are $\boldsymbol{\phi} = \{\phi_{z_c}, \phi_{\boldsymbol{p}^{add}_{base}}, \phi_{\boldsymbol{R}_{base}}, \phi_{\boldsymbol{t}_s}, \phi_{\boldsymbol{p}_{Rc}}, \phi_{\boldsymbol{p}_{Lc}}, \phi_{\boldsymbol{R}_{Rc}}, \phi_{\boldsymbol{R}_{Lc}}\}$, and $\phi_{\boldsymbol{R}_{base}}$ only effects yaw axis rotation. The boundary constraints are set as follows: $0.5 \le \phi_{z_c} \le 1.0$, $-0.2 \le \phi_{p^{add}_{base,i}} \le 0.2$ [m], and $-\pi/2 \le \phi_{R_{base,i}} \le \pi/2$ [rad]. The foot-print parameters $\phi_{\boldsymbol{t}_s}, \phi_{\boldsymbol{p}_{Rc}}, \phi_{\boldsymbol{p}_{Lc}}, \phi_{\boldsymbol{R}_{Rc}}, \phi_{\boldsymbol{R}_{Lc}}$ are initialized to the values measured from reference motion using the method proposed by Miura et al. [5]; and ϕ_{swing} is set to 0.06 m. We used the efficient "L-BFGS-B" method [16] for optimization.

C. Results and discussion

At first, we analyzed the relationship between the cost function and the number of control points of the two B-spline trajectories. Table.I shows the convergence cost values when the set of the target parameter of optimization is changed, and numbers in parentheses are the number of control points of the B-spline trajectory. We confirmed that the error decreased according to the number of control points. According to the analysis, the number of control points of each spline trajectory was finally set to 20, as a result of optimizing the entire 67 dimensional parameters.

TABLE I

CONVERGENCE ERROR VALUES AND THE SET OF OPTIMIZED PARAMETERS.

Optimized parameters ϕ	Total dims	Convergence value
$z_c, \boldsymbol{p}^{add}_{base}(5), \boldsymbol{R}_{base}(5)$	11	7.501×10^{2}
$z_c, \boldsymbol{p}^{add}_{base}(10), \boldsymbol{R}_{base}(10)$	21	7.341×10^{2}
$z_c, \boldsymbol{p}^{add}_{base}(20), \boldsymbol{R}_{base}(20)$	41	7.190×10^{2}
$z_c, \boldsymbol{p}^{add}_{base}(20), \boldsymbol{R}_{base}(20), \boldsymbol{t}_s, \boldsymbol{p}_{Rc}, \boldsymbol{p}_{Lc}, \boldsymbol{R}_{Rc}, \boldsymbol{R}_{Lc}$	67	6.868×10^{2}

To see whether the optimized solution is globally optimal, we tested the four initial values including $\phi_{init} = \phi_{min}$, $\phi_{init} = \phi_{max}$ and $\phi_{init} = (\phi_{max} + \phi_{min})/2$. The variance of the final objective function among 4 cases is less than 2×10^{-10}. This result can be regarded as converging to the neighborhood of the global minimum.

Snapshots of the motion that realized on HRP-4 are shown in Fig.6. As can be seen in the figure, the retargeted motion was performed stably. The optimized CoM trajectory, the waist trajectory, ϕ_{z_c}, and CoM trajectory of the target motion

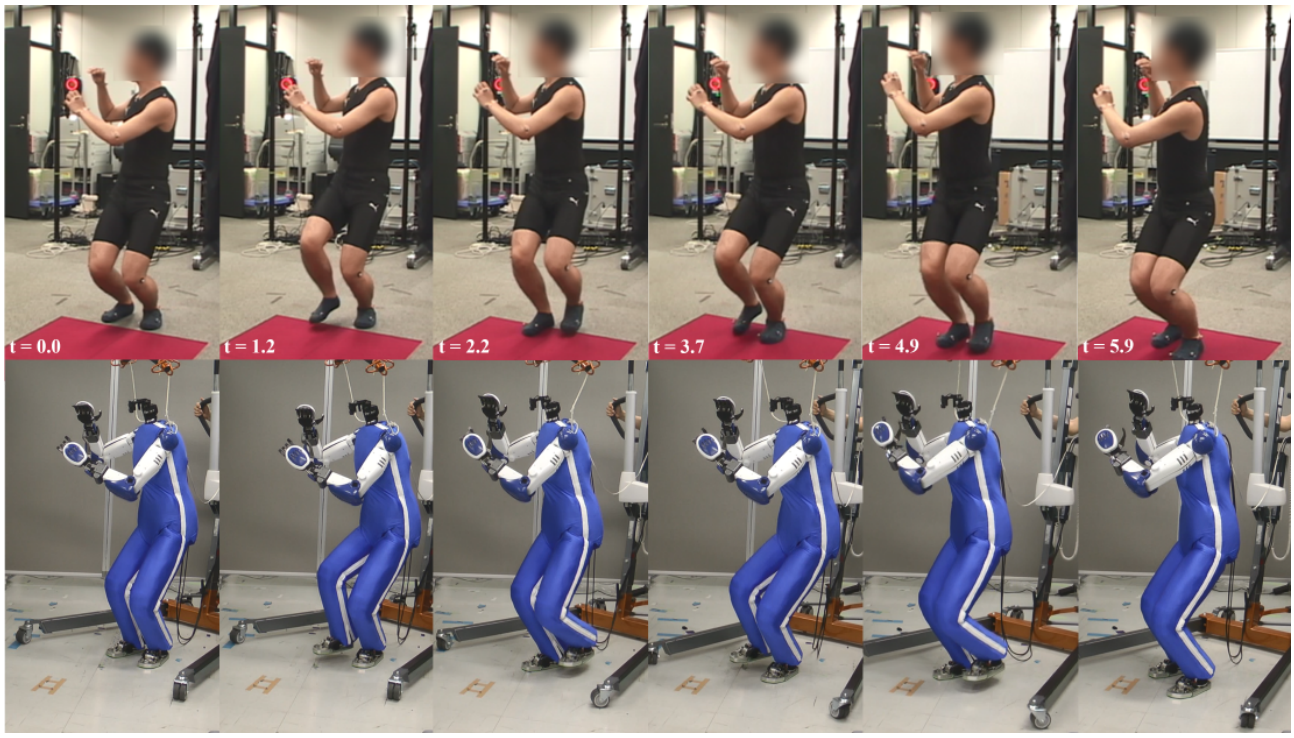

Fig. 6. Original human motion (top) and reproduced motion on HRP-4 (bottom). The motion includes four steps, and the timing of snapshots are the start and end, and each leg swinging.

are shown in Fig.7. The waist vertical movement reproduced the motion feature whereas the CoM trajectory tracks ϕ_{z_c}, which validated the effectiveness of the proposed method. It should be noted that our approach tends to modify CoM trajectory according to the dynamics of LIPM. Therefore, the motion with a large perturbation of CoM is difficult to be retargeted by the proposed method, which will be investigated in our future work.

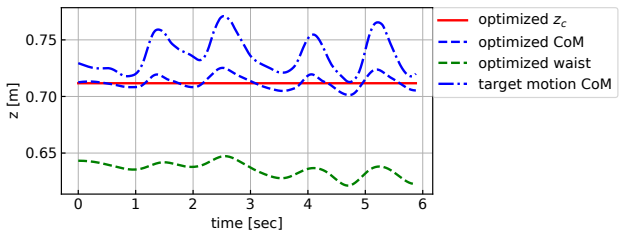

Fig. 7. CoM trajectory, baselink position trajectory and z_c of the generated motion.

Figure 8 shows the joint angle trajectory of the hip yaw, hip roll, hip pitch (θ_{hip}), and knee joint (θ_{knee}) of the reference motion and generated motion. The hip yaw joint and the knee joint were reproduced with high accuracy (in the hip yaw joint, a maximum error is 5° or less); however, there is room for improving the results about other joints. Assuming that the optimization of the $\phi_{\boldsymbol{R}_{base}}$ improved the hip yaw joint, other joints will also improve by optimizing the other axis rotation of the baselink.

V. Conclusions

In this paper, we presented a novel retargeting method for human motions which included the steps taken by a humanoid robot to cope with optimization under the constraints of the complex dynamics and instability induced by the changes in foot placements. We addressed this problem by optimizing the parameters of the LIPM-based walking pattern generator, and minimizing the difference from the reference motion. The implemented pattern generator can generate various motions, and the gradient of all input parameters for the output motion can be computed by the AD technique. Thanks to the efficient and accurate gradient calculation, we could optimize many parameters and reproduce the detailed motion features by determining 67 parameters including the parameter corresponding to the foot-print and the baselink posture trajectory.

The effectiveness of our method was verified by a real-robot experiment supposing a practical inspection task. The proposed method was applied to the motion of working in a half-siting posture, and the reproduced motion was realized by the humanoid HRP-4.

We are also aware of several limitations to our method. The first limitation is related to the stabilizing controller on a real robot. We have constructed a method assuming a stabilizing controller based on the LIPM, but this is a restriction when considering reproduction that uses a wider range of motions. It is necessary to simultaneously improve

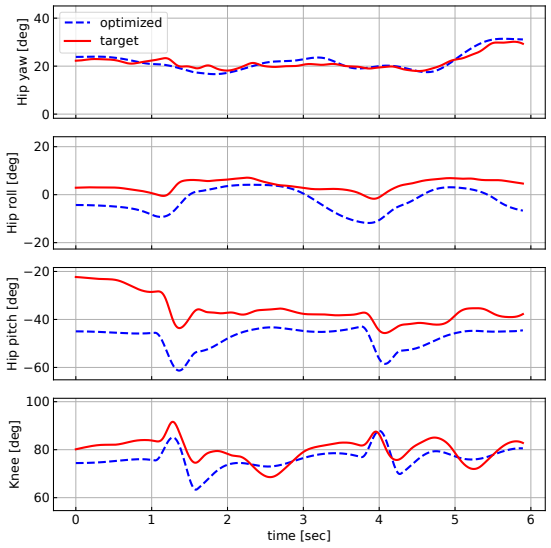

(a) Right leg

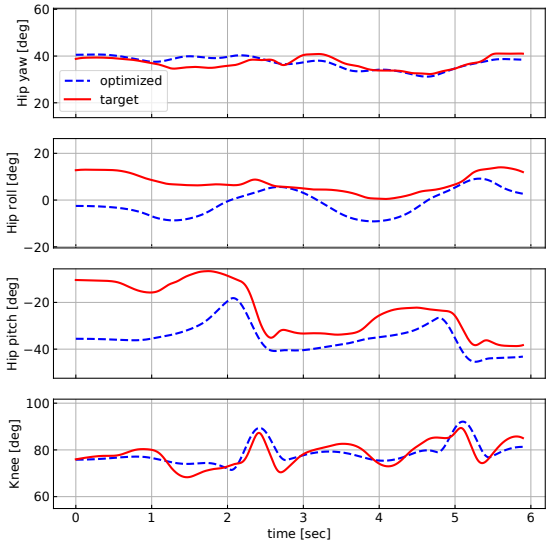

(b) Left leg

Fig. 8. Comparison of the leg joint angle trajectory of the generated motion with reference motion. In each figure shows the hip yaw joint, hip roll joint, hip pitch joint, and knee joint in order from the top.

both the stabilization controller and the retargeting method. The second issue is evaluating the reproducibility of the proposed retargeting method. In this method, it is possible to discuss how much the error decreases with respect to the reference robot motion, but it is still difficult to argue how close it is to the original human motion as a whole; it will be needed when applying this method for evaluation of assistive devices in the future. To deal with this problem, it is necessary to extend our method for characterizing the quantitative features of human likeness in terms of different aspects of kinematics and dynamics, as discussed in [12].

REFERENCES

[1] K. Ayusawa, E. Yoshida, Y. Imamura, and T. Tanaka, "New evaluation framework for human-assistive devices based on humanoid robotics," *Advanced Robotics*, vol. 30, no. 8, pp. 519–534, 2016.

[2] C. Nabeshima, K. Ayusawa, C. Hochberg, and E. Yoshida, "Standard performance test of wearable robots for lumbar support," *IEEE Robotics and Automation Letters*, vol. 3, no. 3, pp. 2182–2189, 2018.

[3] S. Nakaoka, A. Nakazawa, F. Kanehiro, K. Kaneko, M. Morisawa, and K. Ikeuchi, "Task model of lower body motion for a biped humanoid robot to imitate human dances," in *2005 IEEE/RSJ International Conference on Intelligent Robots and Systems*, 2005, pp. 3157–3162.

[4] O. E. Ramos, N. Mansard, O. Stasse, C. Benazeth, S. Hak, and L. Saab, "Dancing humanoid robots: Systematic use of osid to compute dynamically consistent movements following a motion capture pattern," *IEEE Robotics Automation Magazine*, vol. 22, no. 4, pp. 16–26, 2015.

[5] K. Miura, M. Morisawa, S. Nakaoka, F. Kanehiro, K. Harada, K. Kaneko, and S. Kajita, "Robot motion remix based on motion capture data towards human-like locomotion of humanoid robots," in *2009 9th IEEE-RAS International Conference on Humanoid Robots*, 2009, pp. 596–603.

[6] Y. Ishiguro, K. Kojima, F. Sugai, S. Nozawa, Y. Kakiuchi, K. Okada, and M. Inaba, "Bipedal oriented whole body master-slave system for dynamic secured locomotion with lip safety constraints," in *2017 IEEE/RSJ International Conference on Intelligent Robots and Systems*, 2017, pp. 376–382.

[7] K. Yamane and Y. Nakamura, "Dynamics filter-concept and implementation of online motion generator for human figures," *IEEE Transactions on Robotics and Automation*, vol. 19, no. 3, pp. 421–432, jun 2003.

[8] S. Kajita, F. Kanehiro, K. Kaneko, K. Yokoi, and H. Hirukawa, "The 3d linear inverted pendulum mode: a simple modeling for a biped walking pattern generation," in *Proceedings 2001 IEEE/RSJ International Conference on Intelligent Robots and Systems*, vol. 1, 2001, pp. 239–246.

[9] S. Kajita, M. Morisawa, K. Miura, S. Nakaoka, K. Harada, K. Kaneko, F. Kanehiro, and K. Yokoi, "Biped walking stabilization based on linear inverted pendulum tracking," in *2010 IEEE/RSJ International Conference on Intelligent Robots and Systems*, 2010, pp. 4489–4496.

[10] H. Kondo, A. Morishima, Y. Ogura, S. Momoki, J. Shimizu, H. ok Lim, and A. Takanishi, "Algorithm of pattern generation for mimicking disabled person's gait," in *2008 2nd IEEE RAS EMBS International Conference on Biomedical Robotics and Biomechatronics*, 2008, pp. 724–729.

[11] K. Kaneko, F. Kanehiro, M. Morisawa, K. Akachi, G. Miyamori, A. Hayashi, and N. Kanehira, "Humanoid robot HRP-4 - humanoid robotics platform with lightweight and slim body," in *2011 IEEE/RSJ International Conference on Intelligent Robots and Systems*, 2011, pp. 4400–4407.

[12] K. Ayusawa and E. Yoshida, "Motion retargeting for humanoid robots based on simultaneous morphing parameter identification and motion optimization," *IEEE Transactions on Robotics*, vol. 33, no. 6, pp. 1343–1357, 2017.

[13] S. Kajita, F. Kanehiro, K. Kaneko, K. Fujiwara, K. Harada, K. Yokoi, and H. Hirukawa, "Biped walking pattern generation by using preview control of zero-moment point," in *2003 IEEE International Conference on Robotics and Automation*, vol. 2, 2003, pp. 1620–1626 vol.2.

[14] R. Neidinger, "Introduction to automatic differentiation and matlab object-oriented programming," *SIAM Review*, vol. 52, no. 3, pp. 545–563, 2010.

[15] K. Nishiwaki, S. Kagami, Y. Kuniyoshi, M. Inaba, and H. Inoue, "Online generation of humanoid walking motion based on a fast generation method of motion pattern that follows desired zmp," in *IEEE/RSJ International Conference on Intelligent Robots and Systems*, vol. 3, 2002, pp. 2684–2689.

[16] R. Byrd, P. Lu, J. Nocedal, and C. Zhu, "A limited memory algorithm for bound constrained optimization," *SIAM Journal on Scientific Computing*, vol. 16, no. 5, pp. 1190–1208, 1995.